

1                    **Velocity of change in vegetation productivity over northern high latitudes**

2

3    Mengtian Huang<sup>1</sup>, Shilong Piao<sup>1,2</sup>, Ivan A. Janssens<sup>3</sup>, Zaichun Zhu<sup>1</sup>, Tao Wang<sup>2</sup>, Donghai Wu<sup>1</sup>,  
4    Philippe Ciais<sup>1,4</sup>, Ranga B. Myneni<sup>5</sup>, Marc Peaucelle<sup>4,6,7</sup>, Shushi Peng<sup>1</sup>, Hui Yang<sup>1</sup>, Josep  
5    Peñuelas<sup>6,7</sup>

6

7    <sup>1</sup> Sino-French Institute for Earth System Science, College of Urban and Environmental Sciences,  
8    Peking University, Beijing 100871, China.

9    <sup>2</sup> Institute of Tibetan Plateau Research, Chinese Academy of Sciences, Beijing 100085, China.

10   <sup>3</sup> Centre of Excellence PLECO (Plant and Vegetation Ecology), Department of Biology,  
11   University of Antwerp, Universiteitsplein 1, B-2610 Wilrijk, Belgium.

12   <sup>4</sup> Laboratoire des Sciences du Climat et de l'Environnement, CEA CNRS UVSQ, Gif-sur-Yvette  
13   91190, France.

14   <sup>5</sup> Department of Earth and Environment, Boston University, Boston, Massachusetts 02215,  
15   USA.

16   <sup>6</sup> CREAM, Cerdanyola del Vallès, Barcelona 08193, Catalonia, Spain.

17   <sup>7</sup> CSIC, Global Ecology Unit CREAM-CSIC-UAB, Bellaterra, Barcelona 08193, Catalonia,  
18   Spain.

19

20                    Manuscript for *Nature Ecology & Evolution*

21

22 Warming is projected to increase the productivity of northern ecosystems<sup>1-3</sup>. However,  
23 knowledge on whether the displacement of vegetation productivity isolines matches the  
24 northward motion of temperature isolines is still limited. Here, for the first time, we  
25 compared changes in the spatial patterns of vegetation productivity and temperature  
26 using the concept of velocity of change, which is defined as the ratio of temporal changes  
27 in a variable to the spatial gradient of the same variable, making it possible to express  
28 these two variables in the same unit of displacement per time<sup>4-9</sup> (e.g. km yr<sup>-1</sup>). Normalized  
29 Difference Vegetation Index (NDVI) data from 1982 to 2011 was used to calculate the  
30 velocity of vegetation productivity north of 50°N. Our results show that the average  
31 velocity for growing season (GS) NDVI (NDVI<sub>GS</sub>; 2.8±1.1 km yr<sup>-1</sup>) is lower than that for  
32 GS mean temperature (T<sub>GS</sub>; 5.4±1.0 km yr<sup>-1</sup>). About 20% of the study area display larger  
33 velocities of NDVI<sub>GS</sub> than T<sub>GS</sub>, mainly in eastern Europe, northeastern and southern  
34 Siberia, and parts of western Canada. By comparison, in northern Europe, western and  
35 central Siberia, and northeastern Canada (52% of the study area), the NDVI<sub>GS</sub> velocity is  
36 less than half of T<sub>GS</sub> velocity, indicating that the northward motion of productivity isolines  
37 is much slower than that of temperature isolines over the last 30 years. We tentatively  
38 attribute this mismatch between the velocities of vegetation productivity and temperature  
39 to the effects of limited resource availability and vegetation acclimation mechanisms.  
40 Analyses of the velocity of ecosystem productivity from ecosystem model simulations  
41 further suggested that limited nitrogen availability is a crucial obstacle for vegetation to  
42 track the warming trend.

43

44 The Earth's climatic system is experiencing significant warming, which has raised concerns  
45 about the impacts on terrestrial ecosystems<sup>10</sup>. In-situ observations, manipulative experiments,  
46 as well as satellite-derived data have all pointed out that vegetation productivity is sensitive to  
47 temperature change in northern high latitudes<sup>1,11-14</sup>.

48

49 Vegetation can adjust to climate change through relatively fast mechanisms (e.g. adjustment of  
50 phenology or physiology<sup>15,16</sup>) and through slower mechanisms (e.g. phenotypic and genotypic  
51 adaptations, changes in community composition<sup>16</sup>). If climate changes slowly and vegetation  
52 has ample time to adjust, it can be expected that warming would result in a northward shift of  
53 vegetation structure and function in the northern hemisphere. In reality, temperature acclimation  
54 and adaptation of plants<sup>17</sup>, as well as limited resource availability such as nitrogen<sup>18</sup>, may  
55 prevent vegetation productivity change from keeping the same rate as the rapid climate  
56 warming. To the contrary, CO<sub>2</sub> fertilization effects and regional nitrogen deposition may  
57 amplify the greening trend induced by warming temperature<sup>3,19</sup>. Unfortunately, knowledge  
58 about the rate at which vegetation responds to ongoing temperature change is still limited. In  
59 particular, it is not known whether and to what extent change in the spatial displacement of  
60 vegetation productivity isolines during recent decades matches the northward motion of  
61 temperature isolines.

62

63 The concept of velocity of change<sup>9</sup> offers the opportunity to directly compare the ongoing  
64 change in the spatial patterns of temperature and productivity. This concept was first developed  
65 for climate impact research to compare the displacement rate of a forcing variable (e.g.  
66 temperature) with that of an impacted variable (e.g. the occurrence of a given species) by  
67 converting them into the same units<sup>4-9,20</sup> (e.g. km yr<sup>-1</sup>). The velocity of change in a geospatial  
68 variable is the ratio of its temporal change to its local geographical gradient<sup>5-7,21,22</sup>. Imagine, for

69 instance, that the mean spring temperature has increased by  $0.3^{\circ}\text{C}$  over 30 years. At the same  
70 location, a  $1^{\circ}\text{C}$  temperature spatial gradient is observed across a 100 km distance with a south-  
71 to-north decrease in temperature. The velocity of spring temperature change is then  $1\text{ km yr}^{-1}$   
72 for this example (temporal trend of  $0.3^{\circ}\text{C}$  over 30 years, divided by the spatial gradient of  $1^{\circ}\text{C}$   
73 over 100 km).

74

75 In a similar manner, within the boundaries of a biome, we can calculate the velocity of change  
76 in vegetation productivity (also in  $\text{km yr}^{-1}$ ). For each local cell, plant productivity responds to  
77 the changes in ambient environment condition, whether the responses are through changes in  
78 phenology or physiology of plant individuals (in-situ), or changes in community composition  
79 (e.g. shrub expansion). Such changes in productivity for each of the multiple pixels over a  
80 region eventually appear as the movement of productivity isolines at regional scale  
81 (Supplementary Figure 1a). In this case, the velocity of productivity change indicates a  
82 displacement in the isolines of this variable due to changes in productivity in response to climate  
83 change for multiple pixels over a certain region (Supplementary Figure 1b). In another word,  
84 the concept of velocity here quantifies how the spatial pattern of vegetation productivity  
85 changes in response to environmental changes during the study period, with different speeds  
86 and directions for each pixel. For a certain location with a south-to-north decrease in vegetation  
87 productivity, a northward velocity of vegetation productivity of  $1\text{ km yr}^{-1}$  over the past 30 years  
88 would indicate that the current productivity of a certain ecosystem has increased from its value  
89 30 years ago to a higher value today equaling to the past productivity of another ecosystem  
90 which is 30 km ( $1\text{ km yr}^{-1}\times 30\text{ years}$ ) south of the target one. The comparison between the  
91 velocities of change in vegetation productivity and temperature then makes it possible to  
92 identify if the motion of productivity isolines is in the same directions of that of temperature  
93 isolines, or / and if the displacement of productivity isolines is faster/slower than that of

94 temperature isolines. Then we can address the question of whether and to what extent changes  
95 in the spatial pattern of vegetation productivity during recent decades have matched the  
96 displacement of temperature isolines (Supplementary Information S1.1).

97

98 In this study, we mapped for the first time the vector (both velocity and direction) of change in  
99 vegetation productivity calculated using satellite-derived long-term Normalized Difference  
100 Vegetation Index (NDVI). The NDVI dataset covers the period of 1982-2011 and was analyzed  
101 for velocity in the region north of 50°N, where vegetation productivity responds mainly to  
102 temperature changes<sup>23,24</sup>. Productivity velocities were then compared to those of temperature  
103 change (see Methods). To minimize the covariate effects of other environmental variables, our  
104 analyses focused only on the overlap of natural ecosystems (defined following the International  
105 Geosphere-Biosphere Program; see Methods; Supplementary Figure 2) and ecosystems where  
106 productivity is temporally positively ( $p < 0.1$ ) correlated with temperature during the study  
107 period (see Methods; Supplementary Figure 3). This study area represents about 76% of the  
108 vegetated area (annual mean NDVI > 0.1) over the northern high latitudes.

109

110 We first calculated the distribution of the velocities and their directions for the sum of the April  
111 to October growing season (GS) NDVI (NDVI<sub>GS</sub>) and GS mean temperature (T<sub>GS</sub>) over the last  
112 30 years (see Methods). The average NDVI<sub>GS</sub> velocity is  $2.8 \pm 1.1$  km yr<sup>-1</sup> over the study area.  
113 Large NDVI<sub>GS</sub> velocities (>10 km yr<sup>-1</sup>) are found in eastern Europe, northeastern and western  
114 Siberia, and low values (<1 km yr<sup>-1</sup>) in central and eastern Canada as well as western Siberia  
115 (Fig. 1a). In 89% of the study area, the directions of NDVI<sub>GS</sub> vectors are from regions with  
116 higher NDVI<sub>GS</sub> values to those with lower values, with the majority of the study area (55%)  
117 showing a northward movement (Fig. 1c). On average, T<sub>GS</sub> velocity over the study area ( $5.4 \pm 1.0$   
118 km yr<sup>-1</sup>) is nearly twice the NDVI<sub>GS</sub> velocity. The largest T<sub>GS</sub> velocities (>10 km yr<sup>-1</sup>) are

119 observed in northern central and eastern Siberia, parts of Europe, as well as eastern and  
120 northeastern Canada, whereas low values ( $<1 \text{ km yr}^{-1}$ ) are found only in southwestern Canada  
121 (Fig. 1b). Northward  $T_{GS}$  vectors are observed in 71% of the study area (Fig. 1d).

122

123 Comparing the vectors of  $NDVI_{GS}$  and  $T_{GS}$  (see Methods), we found that, across the study area,  
124 91% of the study area show a positive ratio between the velocities of projected  $NDVI_{GS}$  vectors  
125 and the velocities of  $T_{GS}$  vectors ( $V_N:V_T$  ratio) (blue color in Fig. 1e). This suggests that in these  
126 regions, vegetation productivity has tracked the direction of temperature change during the  
127 study period. Among these regions, about 98% of the area show positive trends in both  $NDVI_{GS}$   
128 and  $T_{GS}$ , that is, vegetation productivity has increased where temperature warmed. Only a few  
129 regions in western Canada with positive  $V_N:V_T$  ratio show decreasing  $NDVI_{GS}$  as a result of  
130 decreasing  $T_{GS}$  during the study period (Supplementary Figure 4). Larger  $NDVI_{GS}$  velocities  
131 (projected along the  $T_{GS}$  velocities) than  $T_{GS}$  velocities occur in 20% of the whole study area,  
132 mainly in eastern Europe, northeastern and southern Siberia, as well as parts of western Canada  
133 (Fig. 1e). In about half of the study area, the  $V_N:V_T$  ratio is lower than 0.5, in particular northern  
134 Europe, central Siberia, and northeastern Canada. Similar results are also obtained when using  
135 different climate forcing datasets, when choosing different GS definitions (May to September  
136 or April to September), or when  $NDVI_{GS}$  velocities were compared with those of mean annual  
137 temperature (Supplementary Figure 5; see also Methods).

138

139 Overall, the largest  $V_N:V_T$  ratios are found in relatively warmer regions (Supplementary Figure  
140 6;  $R=0.89$ ,  $p<0.01$ ). Several possible reasons may explain this phenomenon. First, the  
141 ubiquitous  $CO_2$  fertilization effect, which can amplify the warming-induced positive trend of  
142 productivity<sup>3</sup>, is expected to be relatively stronger at higher temperature<sup>25,26</sup>. Second, larger  
143  $V_N:V_T$  ratios in warmer regions may arise from larger nitrogen availability, either from

144 increased soil nitrogen mineralization or from additional nitrogen deposited to ecosystems in  
145 most of the warmer temperate regions of the northern hemisphere<sup>27,28</sup>. In addition, the lower  
146  $V_N:V_T$  ratios found in colder climates may be associated with background limitations induced  
147 from the presence of permafrost (Supplementary Figure 7). Permafrost constrains the  
148 development of roots, and slows down the decompositions of soil organic matter limiting  
149 mineral nitrogen and phosphorus availability for plants<sup>29</sup>.

150

151 In general, vegetation productivity north of 50°N is mainly limited by two factors: growing  
152 season length and growing season maximum photosynthetic capacity<sup>24,30</sup>. Growing season  
153 length is determined by the start of the growing season (SOS) and the end of the growing season  
154 (EOS), which are closely associated with temperature<sup>23</sup>, while peak growing season  
155 photosynthetic capacity can be partly reflected by the maximum NDVI in the growing season  
156 (MOS), which is jointly controlled by nutrient availability and temperature for the study area<sup>31</sup>.  
157 Hence, we analyzed separately the vectors of NDVI-derived SOS, EOS, and MOS, respectively  
158 (see Methods), as shown in Fig. 2.

159

160 The average velocity of change in the SOS date during 1982-2011 is  $3.6 \pm 1.0 \text{ km yr}^{-1}$  over the  
161 study area. Pronounced differences in both velocity and direction of SOS vectors can be seen  
162 between Eurasia and North America in Fig. 2a and 2d, respectively. The majority of Eurasia  
163 (74%) show northward SOS vectors (related to the advance in spring phenology), while only  
164 half of North America display northward SOS vectors (Fig. 2d). In Eurasia, the velocity of SOS  
165 vectors exceeds  $5 \text{ km yr}^{-1}$  in 61% of the whole area, whereas in most of North America (73%  
166 of the continent area north of 50°N), it is lower than  $5 \text{ km yr}^{-1}$  (Fig. 2a). The largest SOS  
167 velocities ( $>20 \text{ km yr}^{-1}$ ) are observed in northeastern Siberia. This area also experiences the  
168 largest ( $>10 \text{ km yr}^{-1}$ ) velocities of springtime (March to May, MAM) temperature increase

169 (Supplementary Figure 8a). In addition, we found that about one third of the study area shows  
170 larger velocities of SOS vectors (projected along the spatial gradient of spring temperature)  
171 than those of spring temperature vectors themselves (Fig. 2g). These regions include central  
172 Europe, central and southern Siberia, as well as parts of eastern and northwestern Canada. By  
173 contrast, in western and northeastern Siberia, the velocities of projected SOS vectors are smaller  
174 than those of the vectors of springtime temperature (ratio<0.5). Moreover, for 17% of the study  
175 area, mainly in Canada, the SOS vectors do not parallel the direction of temperature vectors  
176 (red color in Fig. 2g). In eastern and central Canada, a delayed SOS date occurs with warming,  
177 whereas in western Canada, an earlier SOS date occurs despite the cooling trend of spring  
178 temperature (Supplementary Figure 9a and 10a). Such mismatches may be attributed to changes  
179 in the relationship between heat requirement and chilling accumulation (the duration and/or  
180 sum of cold temperature during dormancy) due to changes in the late-winter and spring  
181 temperature<sup>32-34</sup>.

182

183 It has been reported that the temperature sensitivity of EOS is lower than that of SOS, because  
184 changes in EOS are co-limited by other factors than temperature<sup>31,35,36</sup> (e.g., photoperiod and  
185 soil moisture). At first sight, our analysis of EOS velocities suggests the opposite result: the  
186 average EOS velocity across the study area ( $6.0 \pm 1.1 \text{ km yr}^{-1}$ ) is nearly twice the SOS velocity  
187 ( $3.6 \pm 1.0 \text{ km yr}^{-1}$ ) during 1982-2011. Nearly 60% of the study area display EOS velocities larger  
188 than  $5 \text{ km yr}^{-1}$  (Fig. 2b). However, change in mean temperature from August to October displays  
189 a much higher average velocity ( $7.1 \pm 1.0 \text{ km yr}^{-1}$ ) than that in spring temperature ( $3.7 \pm 1.0 \text{ km}$   
190  $\text{yr}^{-1}$ ), rendering their average warming dependency more similar. In any case, the co-regulation  
191 of EOS by other factors likely explains the much more heterogeneous pattern of the directions  
192 of EOS vectors (Fig. 2e) than that of SOS vectors (Fig. 2d). Comparing EOS and August to  
193 October mean temperature vectors, we found that regions where the velocities of projected EOS



194 vectors exceed those of the original temperature vectors are located mainly in southern Siberia  
195 as well as in northeastern and southwestern Canada, accounting for 36% of the study area (Fig.  
196 2h). By contrast, northeastern Siberia and eastern Canada experience very strong warming  
197 during August-October (Supplementary Figure 10b), but the EOS vectors in these regions show  
198 generally lower velocity than in southeastern Siberia (Fig. 2b), resulting in a smaller ratio ( $<0.5$ )  
199 of EOS to autumn temperature change velocities (Fig. 2h). In parts of central Siberia and  
200 western Canada, we even observe an advanced EOS date with warming temperature (red color  
201 in Fig. 2h). This mismatch between the vectors of EOS and temperature change may be partly  
202 explained by the decreased solar radiation in these regions<sup>36</sup>. Since it has been suggested that  
203 increases in solar radiation suppress the accumulation of abscisic acid and subsequently slow  
204 the speed of leaf senescence<sup>37</sup>, the decline in solar radiation may have resulted in advanced  
205 EOS dates despite the warming temperature.

206

207 On average, the northern high latitudes exhibit an average MOS velocity of  $3.1 \pm 1.0 \text{ km yr}^{-1}$   
208 over the past three decades, which is lower than that of summer (June to July) temperature  
209 ( $4.2 \pm 1.1 \text{ km yr}^{-1}$ ). MOS velocities larger than  $10 \text{ km yr}^{-1}$  are found in eastern Europe,  
210 northeastern Siberia and northeastern Canada, while values lower than  $1 \text{ km yr}^{-1}$  mainly appear  
211 in the southern part of central Siberia, as well as in central and eastern Canada (Fig. 2c).  
212 Comparison between the velocity of MOS vectors (projected along the spatial gradient of  
213 summer temperature) and that of summer temperature vectors (Fig. 2i) show that larger MOS  
214 than temperature change velocities mainly occur in eastern Europe, northeastern Siberia, as well  
215 as in western and northeastern Canada, accounting for one third of the area where changes in  
216 MOS have tracked the direction of the temperature change (blue color in Fig. 2i). In  
217 northwestern Europe and southern Siberia, however, MOS velocities are generally less than  
218 half of summer temperature velocities. Since northern ecosystems are strongly temperature-

219 limited<sup>2</sup>, the slower velocities of projected MOS vectors compared to summer temperature  
220 velocities may be partly attributed to the fact that photosynthesis at the peak of the growing  
221 season is constrained because the low-temperature-induced nutrient limitations do not allow the  
222 development of dense canopies<sup>38</sup>. Interestingly, we found larger MOS velocities in shrub and  
223 tundra ecosystems ( $3.4 \pm 1.0 \text{ km yr}^{-1}$  on average) (vegetation types from the International  
224 Geosphere-Biosphere Program; Supplementary Figure 2) than in other vegetation types. Also  
225 the ratio of velocities of projected MOS vectors to summer temperature velocities is highest in  
226 shrub and tundra (Supplementary Table 1). Warming-induced tall shrub and tree expansion<sup>39</sup>  
227 may be responsible for the larger MOS velocities in shrub and tundra than in other terrestrial  
228 ecosystems.

229

230 Land surface models are used to project future responses of ecosystems to climate change and  
231 to analyze the contribution of different driving factors<sup>40</sup>. We therefore examined the vectors of  
232 change in vegetation productivity using simulated net primary productivity (NPP) from five  
233 process-based land surface models (CLM4.5, LPJG, OCN, ORCHIDEE, and VEGAS; see  
234 Methods and Supplementary Table 2). Our results show that the ensemble model-mean of  
235 change in annual NPP displays an average velocity of  $4.0 \pm 1.3 \text{ km yr}^{-1}$  ( $\pm$ standard deviation  
236 across models). The highest NPP velocity values ( $>10 \text{ km yr}^{-1}$ ) are found in southern and  
237 northeastern Siberia (Supplementary Figure 11a). We next compared the velocities of simulated  
238 NPP with those of NDVI<sub>GS</sub> after projecting both NPP and NDVI<sub>GS</sub> vectors along the spatial  
239 gradient of T<sub>GS</sub> (see Methods). The results show that, on average, about 60% of the study area  
240 (ranging from 47% to 70% across different models) show higher velocities of simulated NPP  
241 than of NDVI<sub>GS</sub>. Further, we examined the NPP velocities using a satellite-derived terrestrial  
242 NPP product (GIMMS<sub>3g</sub> NPP; see Methods), which display spatial patterns consistent with  
243 those of the NDVI<sub>GS</sub> vectors (for both velocity and direction), albeit with generally lower

244 velocity across the study area (Supplementary Figure 12). Compared with the GIMMS<sub>3g</sub> NPP,  
245 the model-simulated NPP produces larger velocity in about 71% (ranging from 61% to 81%) of  
246 the study area. This mismatch regarding the increase in productivity under warming between  
247 model- and satellite-based estimates may partly be explained by the limited availability of  
248 nitrogen in these regions<sup>41</sup>, which is suggested to prevent changes in vegetation productivity  
249 from adequately tracking the warming trend, but are not accounted for in some of the models<sup>42</sup>.  
250 Interestingly, we found that the two models with nitrogen limitations and nitrogen deposition  
251 taken into consideration (CLM4.5 and OCN) both produce lower NPP velocities ( $1.7\pm 1.0$  km  
252  $\text{yr}^{-1}$  and  $2.0\pm 1.1$  km  $\text{yr}^{-1}$  for CLM4.5 and OCN, respectively) than those without a coupled  
253 nitrogen cycle ( $3.5\pm 1.0$  km  $\text{yr}^{-1}$ ,  $2.9\pm 1.1$  km  $\text{yr}^{-1}$  and  $4.7\pm 1.2$  km  $\text{yr}^{-1}$  for LPJG, ORCHIDEE  
254 and VEGAS, respectively) (Supplementary Table 3). Similar results are also observed for gross  
255 primary productivity (GPP; Supplementary Table 3 and Figure 13).

256

257 In summary, in this study we applied the concept of velocity to remotely sensed NDVI fields  
258 and compared the NDVI velocity to that of temperature in northern (predominantly temperature  
259 limited) ecosystems north of 50°N. The average velocity of change in NDVI<sub>GS</sub> ( $2.8\pm 1.1$  km  $\text{yr}^{-1}$ )  
260 over the study area is only about half of that in T<sub>GS</sub> ( $5.4\pm 1.0$  km  $\text{yr}^{-1}$ ). A mismatch between  
261 the NDVI<sub>GS</sub> and T<sub>GS</sub> velocities suggests that the ratio of sensitivities of productivity to  
262 temperature across space and in time is not equal to one (Supplementary Information S2.1).  
263 Our analyses thus combined time and space and to some extent challenged the space-for-time  
264 substitution hypothesis<sup>43</sup> as applied in several studies using spatial gradients to back-cast  
265 temporal changes. Moreover, such a mismatch between productivity and temperature velocities  
266 suggests a disequilibrium in the plasticity of vegetation productivity changes to tail off with the  
267 spatial spread of warming. This may due to the prevalence of background spatial limitations by  
268 other factors limiting vegetation productivity such as soil moisture and nutrients<sup>18</sup>, which also

269 correspond to vegetation acclimation to the ongoing warming<sup>17</sup>, as well as the transient  
270 limitations in the rate of adjustment of plant response to the warming rate in different seasons.  
271 In addition, differences in the magnitudes of the SOS, EOS and MOS velocities suggest that  
272 the seasonal profile of vegetation growth has strongly re-shaped over time and that limitations  
273 may be expected in spring phenology not being able to track temperature moving northward  
274 (e.g. for photoperiod limitations, chilling requirements reasons<sup>32-34</sup>).

275

## 276 **Methods**

277 **Data.** The monthly air temperature data set used in this study is the CRU TS 3.22 climate data  
278 set obtained from Climatic Research Unit (CRU) for the period January 1982 to December 2011  
279 (<http://www.cru.uea.ac.uk/cru/data/hrg/>). We also used WATCH Forcing Data Methodology to  
280 ERA-Interim data with temporal resolution of 3 hour (WFDEI)<sup>44</sup>. The third generation Global  
281 Inventory Monitoring and Modeling System Normalized Difference Vegetation Index (GIMMS  
282 NDVI<sub>3g</sub>) data set from the Advanced Very High Resolution Radiometer (AVHRR) sensors was  
283 downloaded from <http://ecocast.arc.nasa.gov/data/pub/gimms/3g.v0/>. The data set has 15-day  
284 temporal frequency from July 1981 to December 2011 with a spatial resolution of 8 km<sup>45</sup>. Only  
285 positive NDVI values from January 1982 to December 2011 were used in this study. We also  
286 used a 16-day NDVI datasets retrieved using observations from Terra Moderate Resolution  
287 Imaging Spectroradiometer (MODIS) (MODIS NDVI) from February 2000 to July 2012 with  
288 spatial resolutions of 1 km<sup>46</sup> to test the robustness of the analyses conducted with GIMMS  
289 NDVI<sub>3g</sub> data. A 30-year (1982-2011) satellite-derived terrestrial net primary productivity (NPP)  
290 data set presented in a recent study<sup>47</sup>, which was calculated using GIMMS leaf area index (LAI)  
291 and fraction of photosynthetically active radiation absorbed by the vegetation (FPAR) based on  
292 MODIS NPP algorithm<sup>47</sup>, was also used. Note that the spatial structures of the error in the  
293 surfaces of NDVI and temperature may be different due to different approaches to obtain

294 gridded datasets. For example, the NDVI differences between neighboring cells obtained from  
295 composite AVHRR images may be more contrasted than those of climate data being obtained  
296 by interpolation of station data or re-analysis with numerical weather prediction models. To  
297 reduce the effect of fine scale spatial structure in the errors on each surface, all the data have  
298 been regridded into a common  $1^{\circ}\times 1^{\circ}$  grid. A mask is applied whereby grid cells where annual  
299 mean NDVI is less than 0.1 are excluded to remove areas with very low ecosystem productivity.  
300 Vegetation types defined following the International Geosphere-Biosphere Program based on a  
301 MODIS land cover classification  
302 ([http://webmap.ornl.gov/wcsdown/wcsdown.jsp?dg\\_id=10011\\_1](http://webmap.ornl.gov/wcsdown/wcsdown.jsp?dg_id=10011_1)) were used to further remove  
303 hardly natural and non-natural vegetation lands.

304

305 **Satellite-derived indexes of vegetation productivity.** The maximum NDVI value at each  
306 bimonthly time step was used to calculate monthly NDVI in order to minimize the effects of  
307 atmospheric water vapor, non-volcanic aerosols and cloud-cover<sup>45</sup>. The growing season (GS)  
308 NDVI ( $NDVI_{GS}$ ) was calculated as the sum of monthly NDVI values from April to October. GS  
309 defined as May to September and April to September were also used for robustness test. Note  
310 that over the northern high latitudes, calculating  $NDVI_{GS}$  with a predefined period is to some  
311 extent challenging in the boreal regions because of the snow effect. Therefore, we calculated  
312 the percentage of the study area with possible snow effects using the quality flag information of  
313 GIMMS  $NDVI_{3g}$  datasets<sup>45</sup>. To be specific, when regridding the original 8 km ( $\approx 1/12$  degree)  
314 monthly data into a  $1^{\circ}\times 1^{\circ}$  gridded monthly data, a  $1^{\circ}\times 1^{\circ}$  pixel is considered to be affected by  
315 snow in this month if less than 70% pixels within a  $12\times 12$  pixel window have a flag value of 1  
316 or 2 (good value). For each year, a pixel is then considered to be affected by snow if more than  
317 2 months during the predefined growing season (e.g. April-October) is affected by snow.  
318 Finally, we defined regions with snow effects as pixels with more than 9 years showing snow

319 effects during the study period. The results show that regions affected by snow are mainly  
320 located in Alaska, northern Europe and parts of eastern Siberia, accounting for only 12% of the  
321 study area (red color in Supplementary Figure 14).

322

323 Two phenological indexes were derived from GIMMS NDVI<sub>3g</sub> data set: the start of growing  
324 season (SOS, DOY) and the end of growing season (EOS, DOY). The SOS date was calculated  
325 as the averaged SOS date estimated by four different methods: Timesat, Spline, Hants and  
326 Polyfit<sup>48-50</sup>. The EOS date was obtained from the averaged EOS estimated by four different  
327 methods: Hants, Polyfit, Double Logistic and Piecewise Logistic<sup>36</sup>. For each year during 1982-  
328 2011, the maximum NDVI of growing season (MOS) was calculated as the peak NDVI value  
329 among monthly NDVI values during the growing season, which was defined based on the  
330 month when the SOS and EOS date occurred.

331

332 **Model-simulated ecosystem productivity.** We used NPP and gross primary productivity (GPP)  
333 outputs from 1982 to 2011 from five process-based land surface models: CLM4.5, LPJG, OCN,  
334 ORCHIDEE, and VEGAS (see model list in Supplementary Table 2). All models were run  
335 based on the TRENDY inter-comparison protocol during the period 1901-2010 using the same  
336 observed climate drivers from CRU-NCEP Version 4  
337 (<http://dods.extra.cea.fr/data/p529viov/cruncep/>), rising atmospheric CO<sub>2</sub> from the combination  
338 of ice core records and atmospheric observations, and land use change from the Hyde database  
339 (<http://dgvn.ceh.ac.uk/node/21>). NPP and GPP from all the five models were all resampled  
340 into 1°×1° grids.

341

342 **The vector of change.** The vector of change in a certain variable takes both velocity and  
343 direction into consideration. For each pixel, the velocity was defined as the ratio between the

344 30-year temporal trend and the spatial gradient in 30-year means<sup>4,6,9,51</sup>. Temporal trend was  
345 calculated using least squares linear regression for each grid<sup>51</sup>. Spatial gradient was calculated  
346 using a 3×3 grid cell neighborhood based on the average maximum technique<sup>9</sup>. Following  
347 Loarie *et al.*<sup>9</sup>, to convert cell height in latitudinal degrees to km, we used 111.325 km degree<sup>-1</sup>.  
348 To convert cell width in longitudinal degrees to km, we calculated  $\cos\left(\frac{\pi}{180}y\right) 111.325$ , in  
349 which  $y$  is the latitude of the pixel in degrees. We also added a uniformly distributed random  
350 noise to each pixel to decrease the incidence of flat spatial gradients that cause infinite velocity  
351 values<sup>9</sup>. For temperature, a random noise from -0.05 to 0.05 °C was used; for NDVI<sub>GS</sub> and the  
352 maximum NDVI value during growing season (MOS), a random noise from -0.005 to 0.005  
353 was used; for the start / end of the growing season (SOS / EOS), a random noise from -0.05-  
354 0.05 DOY was used; for NPP / GPP, a random noise from -0.5-0.5 gC m<sup>-1</sup> yr<sup>-1</sup> was used. The  
355 direction of each vector was determined from the orientation of the spatial gradient, together  
356 with the direction of change in a particular variable<sup>4</sup>. For example, if temperature showed a  
357 positive trend during the study period, then the direction of temperature vector is towards areas  
358 that used to be cooler. Therefore, assuming a south-to-north decrease in temperature over the  
359 study area, then a northward (that is, along the spatial gradient) temperature vector indicates a  
360 warming temperature during the study period. Similarly, a northward NDVI<sub>GS</sub> vector refers to  
361 an increase in NDVI<sub>GS</sub> during the study period. A northward SOS vector is evidence for an  
362 earlier trend in SOS date, while for EOS, a northward vector is evidence for a delayed EOS  
363 date during the study period. A northward MOS vector is associated with a positive trend of  
364 MOS at the local pixel during the study period.

365

366 We compared the velocity of change in NDVI<sub>GS</sub> derived from GIMMS NDVI<sub>3g</sub> with the one  
367 obtained from MODIS NDVI during 2001-2011. The processing of MODIS NDVI datasets is  
368 based on spectral bands that are specifically designed for vegetation monitoring and take state-

369 of-the-art navigation, atmospheric correction, reduced geometric distortions and improved  
370 radiometric sensitivity into consideration<sup>46</sup>. MODIS NDVI is considered to be an improvement  
371 over the NDVI product derived from the AVHRR sensors<sup>46,52</sup>, but it also has the disadvantage  
372 of shorter time span compared to GIMMS NDVI<sub>3g</sub>. Generally, the NDVI<sub>GS</sub> velocity from  
373 MODIS NDVI shows similar spatial pattern to that from GIMMS NDVI<sub>3g</sub>, even though larger  
374 values of the former than the latter in parts of central, northern and northeastern Canada  
375 (Supplementary Figure 15).

376

377 **Analysis.** This study covered regions where vegetation productivity was temporally  
378 significantly ( $p < 0.1$ ) correlated with temperature from 1982 to 2011. Assuming a linear  
379 relationship between vegetation productivity and temperature, the strength (correlation) of the  
380 linkage between the two variables was determined by the Pearson correlation coefficient  
381 between the time series of NDVI<sub>GS</sub> and GS mean temperature, i.e., between the time series of  
382 the sum of monthly NDVI during April-October and the mean temperature during April-  
383 October. To compare the vectors of vegetation productivity and temperature velocities, for each  
384 grid cell, we calculated the ratio between the velocity of vegetation productivity ( $V_V$ ) along the  
385 spatial gradient of temperature ( $V_V'$ ) and the velocity of temperature ( $V_T$ ). Here  $V_V'$  was  
386 computed as the velocity of the vegetation vector after projecting it along the spatial gradient  
387 of temperature, which can be expressed as  $V_V' = |V_V| \times \cos(|A_T - A_V|)$ , where  $A_T$  and  $A_V$  is the  
388 vector angle (in radians) for metrics of temperature and vegetation productivity, respectively.  
389 The sign of the ratio between  $V_V'$  and  $V_T$  was determined from the directions of both vectors.  
390 For a given pixel, a positive ratio is observed if the vector of change in vegetation productivity  
391 displays the same direction as the vector of temperature change, suggesting that change in the  
392 spatial pattern of vegetation productivity was directionally consistent with that of temperature.  
393 A negative ratio indicates that the directional change in the spatial patterns of the two variables



394 were of opposite directions. The NDVI<sub>GS</sub> vector was compared with the vector of GS mean  
395 temperature with different definitions of GS: April to October, May to September, and April to  
396 September. Comparisons of vector of NDVI<sub>GS</sub> and that of mean annual temperature were also  
397 presented. Since the timing of vegetation phenology is associated with temperature of the  
398 preceding 0-3 months<sup>36,53</sup>, here the vector of change in the SOS and EOS date were compared  
399 with that of change in mean temperature during March to May and August to October,  
400 respectively. The vector of change of MOS was compared with that of change in mean  
401 temperature during June to July. Note that since it has been well recognized that increasing  
402 spring temperature (i.e. positive trend of temperature) tends to result in an earlier SOS date (i.e.  
403 negative trend of SOS date) over most of northern ecosystems during the past three decades<sup>54</sup>,  
404 regions where the change in vegetation productivity were consistent with warming trend refer  
405 to those with a negative trend in SOS date during the study period. The vectors of change in  
406 satellite-derived NPP, as well as model-simulated annual NPP and GPP were calculated using  
407 the same methods as calculating NDVI<sub>GS</sub> vectors, and compared with the vector of change in  
408 GS (April to October) mean temperature.

409

## 410 **References**

- 411 1 Elmendorf, S. C. *et al.* Plot-scale evidence of tundra vegetation change and links to  
412 recent summer warming. *Nat. Clim. Chang.* **2**, 453-457 (2012).
- 413 2 Nemani, R. R. *et al.* Climate-driven increases in global terrestrial net primary  
414 production from 1982 to 1999. *Science* **300**,1560-1563 (2003).
- 415 3 Zhu, Z. *et al.* Greening of the Earth and its drivers. *Nat Clim Chang* **6**, 791-795 (2016).
- 416 4 Ackerly, D. *et al.* The geography of climate change: implications for conservation  
417 biogeography. *Divers. Distrib.* **16**, 476-487 (2010).

- 418 5 Burrows, M. T. *et al.* The pace of shifting climate in marine and terrestrial ecosystems.  
419 *Science* **334**, 652-655 (2011).
- 420 6 Burrows, M. T. *et al.* Geographical limits to species-range shifts are suggested by  
421 climate velocity. *Nature* **507**, 492-495 (2014).
- 422 7 Diffenbaugh, N. S. & Field C. B. Changes in ecologically critical terrestrial climate  
423 conditions. *Science* **341**, 486-492 (2013)
- 424 8 Dobrowski, S. Z. *et al.* The climate velocity of the contiguous United States during the  
425 20th century. *Glob. Chang Biol.* **19**, 241-251 (2013).
- 426 9 Loarie, S. R. *et al.* The velocity of climate change. *Nature* **462**, 1052-1055 (2009).
- 427 10 Parry, M. L. *Climate change 2007-impacts, adaptation and vulnerability: Working*  
428 *group II contribution to the fourth assessment report of the IPCC*, Cambridge University  
429 Press (2007).
- 430 11 Buitenwerf, R., Rose, L. & Higgins, S. I. Three decades of multi-dimensional change in  
431 global leaf phenology. *Nat. Clim. Chang.* **5**, 364-368 (2015).
- 432 12 Vitisse, Y., Porté, A. J., Kremer, A., Michalet, R. & Delzon, S. Responses of canopy  
433 duration to temperature changes in four temperate tree species: relative contributions of  
434 spring and autumn leaf phenology. *Oecologia* **161**, 187-198 (2009).
- 435 13 Wolkovich, E. M. *et al.* Warming experiments underpredict plant phenological  
436 responses to climate change. *Nature* **485**, 494-497 (2012).
- 437 14 Wu, Z., Dijkstra, P., Koch, G. W., Peñuelas, J. & Hungate B. A. Responses of terrestrial  
438 ecosystems to temperature and precipitation change: a meta-analysis of experimental  
439 manipulation. *Glob. Chang Biol.* **17**, 927-942 (2011).

- 440 15 Peñuelas, J. & Filella, I. Responses to a warming world. *Science* **294**, 793-795 (2001).
- 441 16 Penuelas, J. *et al.* Evidence of current impact of climate change on life: a walk from  
442 genes to the biosphere. *Glob. Chang Biol.* **19**, 2303-2338 (2013).
- 443 17 Hikosaka, K., Ishikawa, K., Borjigidai, A., Muller, O. & Onoda, Y. Temperature  
444 acclimation of photosynthesis: mechanisms involved in the changes in temperature  
445 dependence of photosynthetic rate. *J. Exp. Bot.* **57**, 291-302 (2006).
- 446 18 Way, D. A. & Oren, R. Differential responses to changes in growth temperature between  
447 trees from different functional groups and biomes: a review and synthesis of data. *Tree*  
448 *Physiol.* **30**, 669-688 (2010).
- 449 19 Thomas, R. Q., Canham, C. D., Weathers, K. C. & Goodale, C. L. Increased tree carbon  
450 storage in response to nitrogen deposition in the US. *Nat. Geosci.* **3**, 13-17 (2010).
- 451 20 Sandel, B. *et al.* The influence of Late Quaternary climate-change velocity on species  
452 endemism. *Science* **334**, 660-664 (2011).
- 453 21 Bi, J., Xu, L., Samanta, A., Zhu, Z. & Myneni, R. Divergent arctic-boreal vegetation  
454 changes between North America and Eurasia over the past 30 years. *Remote Sens.* **5**,  
455 2093-2112 (2013).
- 456 22 LoPresti, A. *et al.* Rate and velocity of climate change caused by cumulative carbon  
457 emissions. *Environ. Res. Lett.* **10**, 095001 (2015).
- 458 23 Lucht, W. *et al.* Climatic control of the high-latitude vegetation greening trend and  
459 Pinatubo effect. *Science* **296**, 1687-1689 (2002).
- 460 24 Myneni, R. B., Keeling, C. D., Tucker, C. J., Asrar, G. & Nemani, R. R. Increased plant  
461 growth in the northern high latitudes from 1981 to 1991. *Nature* **386**, 698-702 (1997).

- 462 25 Hickler, T. *et al.* CO<sub>2</sub> fertilization in temperate FACE experiments not representative of  
463 boreal and tropical forests. *Glob. Chang Biol.* **14**, 1531-1542 (2008).
- 464 26 Schimel, D., Stephens, B. B. & Fisher, J. B. Effect of increasing CO<sub>2</sub> on the terrestrial  
465 carbon cycle. *Proc. Natl. Acad. Sci. U.S.A.* **112**, 436-441 (2015).
- 466 27 Granath, G. *et al.* Photosynthetic performance in Sphagnum transplanted along a  
467 latitudinal nitrogen deposition gradient. *Oecologia* **159**, 705-715 (2009).
- 468 28 Livingston, N., Guy, R., Sun, Z. & Ethier, G. The effects of nitrogen stress on the stable  
469 carbon isotope composition, productivity and water use efficiency of white spruce  
470 (*Picea glauca* (Moench) Voss) seedlings. *Plant Cell Environ.* **22**, 281-289 (1999).
- 471 29 Kimball, J. S. *et al.* Recent climate-driven increases in vegetation productivity for the  
472 western arctic: evidence of an acceleration of the northern terrestrial carbon cycle. *Earth*  
473 *Interact.* **11**, 1-30 (2007).
- 474 30 Xia, J. *et al.* Joint control of terrestrial gross primary productivity by plant phenology  
475 and physiology. *Proc. Natl. Acad. Sci. U.S.A.* **112**, 2788-2793 (2015).
- 476 31 Forkel, M. *et al.* Codominant water control on global interannual variability and trends  
477 in land surface phenology and greenness. *Glob. Chang Biol.* **21**, 3414-3435 (2015).
- 478 32 Fu, Y. H. *et al.* Declining global warming effects on the phenology of spring leaf  
479 unfolding. *Nature* **526**, 104-107 (2015).
- 480 33 Laube, J. *et al.* Chilling outweighs photoperiod in preventing precocious spring  
481 development. *Glob. Chang Biol.* **20**, 170-182 (2014).
- 482 34 Zhang, X., Tarpley, D. & Sullivan, J. T. Diverse responses of vegetation phenology to a  
483 warming climate. *Geophys. Res. Lett.* **34**, L19405 (2007).

484 35 Barichivich, J. *et al.* Large-scale variations in the vegetation growing season and annual  
485 cycle of atmospheric CO<sub>2</sub> at high northern latitudes from 1950 to 2011. *Glob. Chang*  
486 *Biol.* **19**, 3167-3183 (2013).

487 36 Liu, Q. *et al.* Temperature, precipitation, and insolation effects on autumn vegetation  
488 phenology in temperate China. *Glob. Chang Biol.* **22**, 644-655 (2016).

489 37 Gepstein, S. & Thimann, K. V. Changes in the abscisic acid content of oat leaves during  
490 senescence. *Proc. Natl. Acad. Sci. U.S.A.* **77**, 2050-2053 (1980).

491 38 Melillo, J. M. *et al.* Soil warming, carbon-nitrogen interactions, and forest carbon  
492 budgets. *Proc. Natl. Acad. Sci. U.S.A.* **108**, 9508-9512 (2011).

493 39 Frost, G. V. & Epstein, H. E. Tall shrub and tree expansion in Siberian tundra ecotones  
494 since the 1960s. *Glob. Chang Biol.* **20**, 1264-1277 (2014).

495 40 Sitch, S. *et al.* Evaluation of the terrestrial carbon cycle, future plant geography and  
496 climate-carbon cycle feedbacks using five Dynamic Global Vegetation Models  
497 (DGVMs). *Glob. Chang Biol.* **14**, 2015-2039 (2008).

498 41 Fisher, J. B., Badgley, G. & Blyth, E. Global nutrient limitation in terrestrial vegetation.  
499 *Glob. Biogeochem. Cycles* **26**, GB1014 (2012).

500 42 Likens G. *Long-term Studies in Ecology* (Springer, 1989).

501 43 Smith, N. G. & Dukes, J. S. Plant respiration and photosynthesis in global-scale models:  
502 incorporating acclimation to temperature and CO<sub>2</sub>. *Glob. Chang Biol.* **19**, 45-63 (2013).

503 44 Weedon, G. P. *et al.* The WFDEI meteorological forcing data set: WATCH Forcing Data  
504 methodology applied to ERA-Interim reanalysis data. *Water. Resour. Res.* **50**, 7505-  
505 7514 (2014).

506 45 Pinzon, J. E. & Tucker, C. J. A non-stationary 1981–2012 AVHRR NDVI3g time series.  
507 *Remote Sens.* **6**, 6929-6960 (2014).

508 46 Huete, A. *et al.* Overview of the radiometric and biophysical performance of the MODIS  
509 vegetation indices. *Remote Sens. Environ.* **83**, 195-213 (2002).

510 47 Smith, W. K. *et al.* Large divergence of satellite and Earth system model estimates of  
511 global terrestrial CO<sub>2</sub> fertilization. *Nat. Clim. Chang.* **6**, 306-310 (2016).

512 48 Cong, N. *et al.* Changes in satellite-derived spring vegetation green-up date and its  
513 linkage to climate in China from 1982 to 2010: a multimethod analysis. *Glob. Chang*  
514 *Biol.* **19**, 881-891 (2013).

515 49 Piao, S., Fang, J., Zhou, L., Ciais, P. & Zhu, B. Variations in satellite-derived phenology  
516 in China's temperate vegetation. *Glob. Chang Biol.* **12**, 672-685 (2006).

517 50 White, M. A. *et al.* Intercomparison, interpretation, and assessment of spring phenology  
518 in North America estimated from remote sensing for 1982-2006. *Glob. Chang Biol.* **15**,  
519 2335-2359 (2009).

520 51 Zheng, B., Chenu, K. & Chapman, S. C. Velocity of temperature and flowering time in  
521 wheat-assisting breeders to keep pace with climate change. *Glob. Chang Biol.* **22**, 921-  
522 933 (2016).

523 52 Fensholt, R. & Proud, S. R. Evaluation of earth observation based global long term  
524 vegetation trends-Comparing GIMMS and MODIS global NDVI time series. *Remote*  
525 *Sens. Environ.* **119**, 131-147 (2012).

526 53 Piao, S. *et al.* Leaf onset in the northern hemisphere triggered by daytime temperature.  
527 *Nat. Commun.* **6**, 6911 (2015).

528 54 Jeong, S., Ho, C. H., Gim, H. J. & Brown, M. E. Phenology shifts at start vs. end of  
529 growing season in temperate vegetation over the Northern Hemisphere for the period  
530 1982–2008. *Glob. Chang Biol.* **17**, 2385-2399 (2011).

531

### 532 **Acknowledgements**

533 This study was supported by National Natural Science Foundation of China (41530528), and  
534 the 111 Project (B14001). IJ, PC, and JP were supported by the European Research Council  
535 Synergy grant SyG-2013-610028 IMBALANCE-P

536

### 537 **Author contributions**

538 S.L.P. designed research; M.T.H. performed analysis; and all authors contributed to the  
539 interpretation of the results and the writing of the paper.

540

### 541 **Author Information**

542 Reprints and permissions information is available at [www.nature.com/reprints](http://www.nature.com/reprints). The authors  
543 have no competing financial interests. Correspondence and requests for materials should be  
544 addressed to S.L.P. ([slpiao@pku.edu.cn](mailto:slpiao@pku.edu.cn))

545

546

547 **Figure Legends**

548 **Figure 1 | The velocity of vegetation productivity (NDVI<sub>GS</sub>) and temperature (T<sub>GS</sub>) from**  
549 **1982 to 2011 over northern high latitudes (north of 50°N). a,** The spatial pattern of the  
550 velocity of the vector of change in NDVI<sub>GS</sub>. **b,** The spatial pattern of the velocity of the vector  
551 of change in T<sub>GS</sub>. **c,** The spatial pattern of the direction of the vector of change in NDVI<sub>GS</sub>. **d,**  
552 The spatial pattern of the direction of the vector of change in T<sub>GS</sub>. **e,** The comparison between  
553 velocity of NDVI<sub>GS</sub> vector after projecting along the spatial gradient of T<sub>GS</sub> and the velocity of  
554 T<sub>GS</sub> vector (see Methods). The growing season is defined as from April to October. The velocity  
555 was calculated as the ratio between the 30-year temporal trend and the spatial gradient in 30-  
556 year means (see Methods). The velocities shown in panel **a** and **b** are original velocities without  
557 projecting the NDVI<sub>GS</sub> vectors along the temperature gradient. For panel **c** and **d**, ‘N’, ‘NE’,  
558 ‘E’, ‘ES’, ‘S’, ‘SW’, ‘W’ and ‘NW’ in the legend refer to ‘North-ward’, ‘Northeast-ward’,  
559 ‘East-ward’, ‘Southeast-ward’, ‘South-ward’, ‘Southwest-ward’, ‘West-ward’, and ‘Northwest-  
560 ward’, respectively. For panel **e**, the ratio between the velocity of NDVI<sub>GS</sub> along the spatial  
561 gradient of T<sub>GS</sub> and the velocity of T<sub>GS</sub> was calculated after projecting NDVI<sub>GS</sub> vector along the  
562 spatial gradient of T<sub>GS</sub> for each pixel (see Methods). A blue color (positive ratio) suggests that  
563 change in the spatial pattern of NDVI<sub>GS</sub> was directionally consistent with the direction of  
564 change in the spatial pattern of T<sub>GS</sub>, while a red color (negative ratio) indicates that the former  
565 was inconsistent with the direction of the latter. Note that only gridded pixels covered by natural  
566 vegetation (defined following the International Geosphere-Biosphere Program based on a  
567 MODIS land cover classification; Supplementary Figure 2) with annual mean NDVI value  
568 larger than 0.1 are shown here.

569

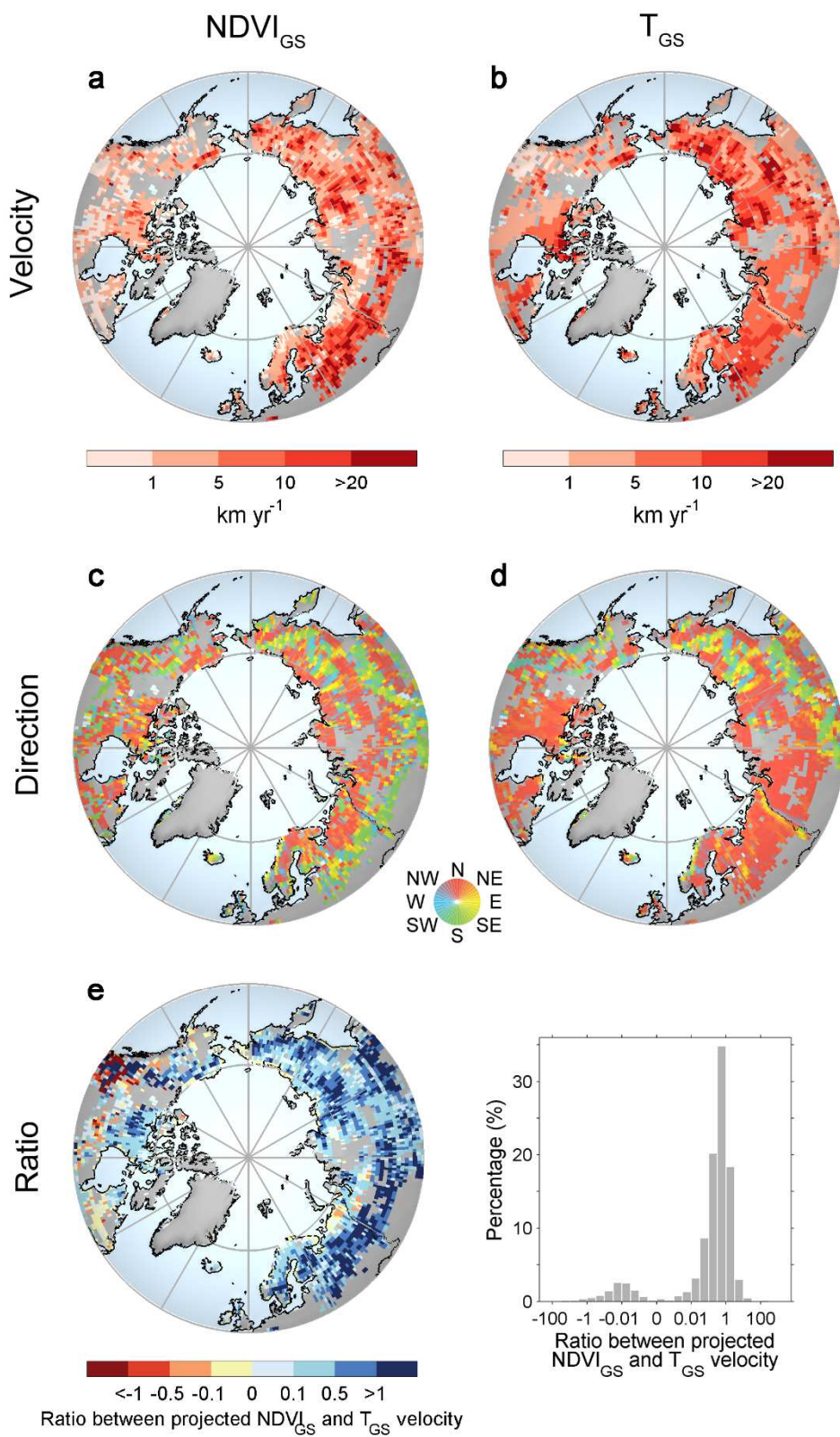
570 **Figure 2 | The velocity (a-c) and direction (d-f) of the vector of change in vegetation**  
571 **phenology and physiology over the northern high latitudes (north of 50 °N) from 1982 to**



572 **2011 and comparison with the velocity of corresponding temperature metrics (g-i).**

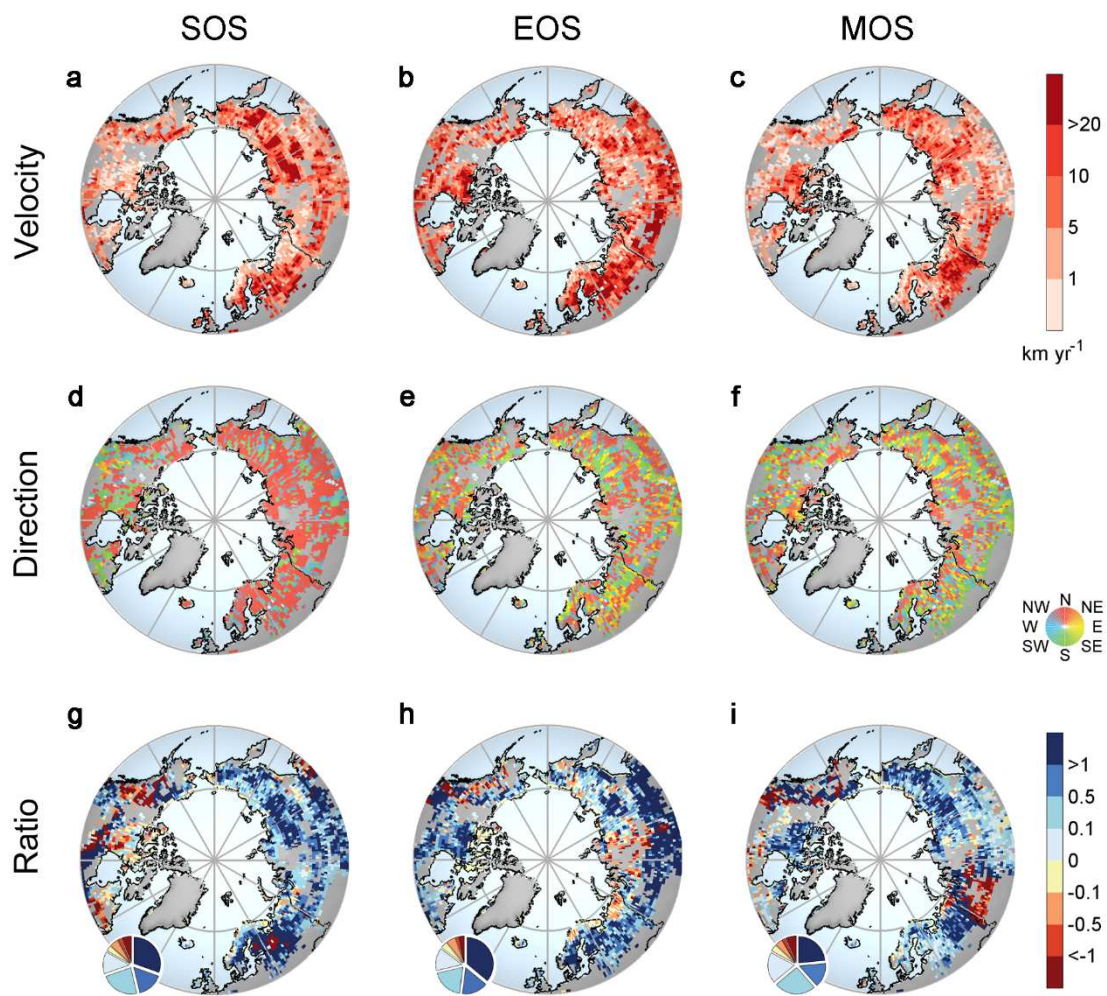
573 Vegetation phenology is characterized by the start of the growing season (SOS) and end of the  
574 growing season (EOS); vegetation physiology is characterized by the maximum NDVI of  
575 growing season (MOS). For each pixel, the velocity for a certain variable was calculated as the  
576 ratio between the 30-year temporal trend and the spatial gradient in 30-year means for each  
577 index (see Methods). The velocities shown in panel **a-c** are original velocities without  
578 projecting the vegetation vectors along the temperature gradient. ‘N’, ‘NE’, ‘E’, ‘ES’, ‘S’, ‘SW’,  
579 ‘W’ and ‘NW’ in the legend for panel **d-f** refer to ‘North-ward’, ‘Northeast-ward’, ‘East-ward’,  
580 ‘Southeast-ward’, ‘South-ward’, ‘Southwest-ward’, ‘West-ward’, and ‘Northwest-ward’,  
581 respectively. For panel **g-i**, the ratio between the velocity of SOS/EOS/MOS along the spatial  
582 gradient of temperature and the velocity of temperature change was calculated after projecting  
583 the vectors of change in SOS/EOS/MOS along the spatial gradient of corresponding  
584 temperature metric for each pixel (see Methods). A blue color (positive ratio) suggests that  
585 change in the spatial pattern of SOS/EOS/MOS was directionally consistent with the direction  
586 of change in the spatial pattern of corresponding temperature metric, while a red color (negative  
587 ratio) indicates that the former was inconsistent with the direction of the latter. Pie chart of  
588 ratios shown in the spatial patterns is shown in the inset at bottom-left of panel **g-i**. Note that  
589 only gridded pixels covered by natural vegetation (defined following the International  
590 Geosphere-Biosphere Program based on a MODIS land cover classification; Supplementary  
591 Figure 2) with annual mean NDVI value larger than 0.1 are shown here.

592



594

595



597

598